Liquidus Phase Relations in the System $CaO–MgO–Al_2O_3–SiO_2$ at 2·0 GPa: Applications to Basalt Fractionation, Eclogites, and Igneous Sapphirine

T.-C. LIU[1] AND D. C. PRESNALL[2]*

[1]DEPARTMENT OF EARTH SCIENCES, NATIONAL TAIWAN NORMAL UNIVERSITY, TAIPEI 117, TAIWAN

[2]MAGMALOGY LABORATORY, DEPARTMENT OF GEOSCIENCES, UNIVERSITY OF TEXAS AT DALLAS, RICHARDSON, TX 75083-0688, USA

RECEIVED NOVEMBER 2, 1998; REVISED TYPESCRIPT ACCEPTED JUNE 14, 1999

To model magmatic crystallization processes for mafic to intermediate compositions at high pressure, liquidus phase relations in the forsterite–anorthite–diopside–silica (FADS) tetrahedron within the $CaO–MgO–Al_2O_3–SiO_2$ system have been determined at 2·0 GPa. Compositions of five liquidus invariant points have been determined and the approximate compositions of five others have been inferred. These involve primary phase volumes for forsterite (fo), enstatite (en), diopside (di), high quartz (qz), spinel (sp), sapphirine (sa), garnet (gt), anorthite (an), and corundum (cor). The determined (with wt % coefficients) and inferred reactions (without coefficients) that define each isobaric invariant point are as follows:

23 en + 68 di + 9 sp = 84 liq + 16 fo
37 di + 63 sa = 47 liq + 40 sp + 13 en
100 gt = 21 liq + 27 sa + 55 en + 18 di
1 di + 59 en + 41 an = 43 liq + 57 gt
18 di + 21 qz + 15 en + 47 an = 100 liq
di + an + gt = liq + sa
an + gt = liq + sa + en
sa + an + di = liq + sp
sa + an = liq + cor + sp
di + cor = liq + an + sp.

These phase relations provide a diverse range of constraints on igneous processes at pressures near 2 GPa. They show that fractional crystallization of a model basalt gives a residual liquid strongly enriched in SiO_2, strongly depleted in MgO, and mildly enriched in Al_2O_3. Such a trend is consistent with the calc-alkaline fractionation trend observed at subduction zones, but is in disagreement with suggestions that fractionation of tholeiitic basalt in this pressure range yields an alkalic basalt. Both trends may occur for natural basalts depending on the Na_2O content of the parental magma. Also, the data show that the minimum pressure for the formation of cumulate eclogites and garnet pyroxenites is about 1·8–1·9 GPa. The lower limit of pressure at which sapphirine can crystallize from a liquid in the FADS tetrahedron is estimated to be 1·1–1·5 GPa and the upper limit is >3 GPa. Sapphirine crystallizes from magmas intermediate in composition between basalt and andesite. Probable igneous sapphirine in mafic associations is rare, but it occurs as part of a pyroxenite xenolith from Delegate, Australia, that we suggest is a cumulate assemblage and in a sapphirine norite at Wilson Lake, Labrador, Canada.

KEY WORDS: *basalt; eclogite; sapphirine; fractional crystallization*

INTRODUCTION

Liquidus phase relations in the system $CaO–MgO–Al_2O_3–SiO_2$ (CMAS) have been used extensively to model the generation and crystallization of basaltic magmas and the crystallization behavior of magma oceans. The portion of this system most relevant to the petrogenesis of mafic and ultramafic magmas is the tetrahedron forsterite–Ca Tschermak's molecule–

*Corresponding author.

diopside–silica, which is a simplified analog of the basalt tetrahedron of Yoder & Tilley (1962). The smaller tetrahedral volume, forsterite–anorthite–diopside–silica (FADS), is an approximation of the tholeiitic portion of the basalt tetrahedron and various parts of this tetrahedron have been the object of many experimental investigations at high pressures. These studies have led to a reasonably good understanding of the broad outline of liquidus phase relations in the interior of the FADS tetrahedron at 1 atm (Presnall *et al.*, 1979; Longhi, 1987) and 3·0 GPa (Milholland & Presnall, 1998), but liquidus phase boundaries at 2·0 GPa have not been determined except for the liquid composition at the invariant point, forsterite + enstatite + diopside + spinel + liquid (Presnall *et al.*, 1979; Walter & Presnall, 1994).

We have determined or inferred the locations of liquidus invariant points and univariant curves throughout the entire tetrahedron. The phase relations are complex, mainly because of the unexpected discovery of primary phase volumes for sapphirine and garnet. These data provide a basis for discussing in general terms the fractional crystallization of model basaltic magmas at 2·0 GPa. The discussion is necessarily limited to the four oxides present in the system, but these oxides make up about 85% of the composition of typical tholeiitic basalts. Sapphirine has been considered to be an almost exclusively metamorphic mineral, but we present evidence here that it would be expected to crystallize from ordinary magmas of intermediate composition between basalt and andesite at high pressures. Also, we use our data to place an approximate lower limit on the pressure at which eclogite and garnet pyroxenite cumulates can form.

Table 1: Compositions of starting mixtures (wt %)

Mixture	Di	An	Fo	En	Qz
60An40En		60·00		40·00	
80An20En		80·00		20·00	
AFQ-20		55·00	20·00		25·00
AFQ-21		53·00	38·00		9·00
AFQ-22		50·00	42·00		8·00
AFQ-23		65·00	8·00		27·00
AFQ-25		72·00	19·00		9·00
AFQ-26		70·00	4·00		26·00
AFQ-28		72·00	14·00		14·00
AED-52	15·00	65·00		20·00	
AED-54	15·00	55·00		30·00	
GS-0		55·00	35·00		10·00
GS-6		60·00	12·00		28·00
GS-8		62·00	22·00		16·00
GS-11		64·00	23·00		13·00
CMAS-4	16·56	52·44	22·83		8·17
CMAS-5	14·86	49·82	28·19		7·13
CMAS-7	21·00	48·00		31·00	
CMAS-10	12·03	55·79	17·91		14·27
CMAS-11	27·48	42·64	12·30		17·58
CMAS-12	6·00	58·00	12·00		24·00
CMAS-13	20·89	47·52	26·70		4·89
CMAS-14	12·69	67·65	10·09		9·57
CMAS-15	7·39	59·76	17·67		15·18
CMAS-16	5·61	57·38	19·13		17·88
CMAS-17	15·02	49·72	29·75		5·51
CMAS-18	9·99	58·51	24·75		6·75
CMAS-19	17·04	62·65	11·60		8·71
CMAS-20	17·89	48·66	27·44		6·01
CMAS-21	7·00	63·39	16·60		13·01
CMAS-22	5·21	61·48	18·10		15·21

Abbreviations: Di, $CaMgSi_2O_6$; An, $CaAl_2Si_2O_8$; Fo, Mg_2SiO_4; En, $MgSiO_3$; Qz, SiO_2.

EXPERIMENTAL METHODS

The starting mixtures (Table 1) are those used by Presnall (1976), Presnall *et al.* (1979), Sen & Presnall (1984) and Liu & Presnall (1990), plus several new mixtures prepared according to the procedures described by Presnall (1966) and Presnall *et al.* (1972). Experiments were performed with piston–cylinder presses (Boyd & England, 1960), and the experimental techniques are the same as described by Liu & Presnall (1990).

Phases in run products were identified microscopically in reflected light. Characteristic relief, reflectivity, and crystal habit were used for phase identification with verification by back-scattered electron imaging or microprobe analysis when necessary. Compositions of glass, enstatite, diopside, garnet, and sapphirine were determined using the JEOL JXA-733 electron microprobe at Southern Methodist University. Most grains chosen for analysis were larger than 10 μm. Glass regions or pools chosen for analysis have dimensions usually larger than 30 μm. Operating conditions and standards used for analysis are the same as described by Liu & Presnall (1990). We have accepted analyses of phases that have sums between 99 and 101 wt % and have structural formulae with 3·96–4·04 cations per six oxygens (pyroxenes), 7·94–8·06 cations per eight oxygens (garnet), or 13·95–14·05 cations per 20 oxygens (sapphirine).

Several workers have pointed out that glass compositions can be significantly altered by the formation of quench crystals (Cawthorn *et al.*, 1973; Green, 1973; Jaques & Green, 1979, 1980). In our experiments, we have found that this is a problem only when attempting to analyze a glass within a few microns of quench crystals.

All of the glass compositions we report here are consistent with results of quenching experiments that bracket the univariant lines. Therefore, we believe these glass compositions are valid in helping to constrain the locations of univariant lines.

Run durations for each primary phase field except corundum were set according to the times established by reversal experiments of Chen & Presnall (1975), Presnall (1976), Presnall *et al.* (1978), Sen & Presnall (1984), Liu & Presnall (1990), and Milholland & Presnall (1998). Two experiments (Table 2) contain corundum, and as equilibria involving corundum have never been reversed in this laboratory, these runs must be considered as synthesis data.

DATA

Table 2 lists quenching experiments using the starting compositions given in Table 1. Electron microprobe determinations of phase compositions are listed in Tables 3 (glass), 4 (enstatite), 5 (diopside), 6 (garnet), and 7 (sapphirine).

In Tables 4 and 5, it can be seen that the pyroxenes show a wide range of Al_2O_3 content from about 10% up to 14·5% for enstatite and 16% for diopside. We find no evidence for the existence of pigeonitic clinopyroxene in equilibrium with liquids well inside the FADS tetrahedron similar to the pyroxenes reported by Kushiro (1969) in equilibrium with liquids on the forsterite–diopside–silica face. Therefore, the primary phase volume for this phase must extend into the tetrahedron only a short distance, but we have no data that define its boundaries.

The sapphirine compositions are of some interest because this mineral is normally of metamorphic rather than igneous origin. Sapphirine shows solid solution by the substitution, $R^{2+} + Si = 2R^{3+}$, mainly between the compositions $2MgO.2Al_2O_3.SiO_2$ (2:2:1) and $7MgO.9Al_2O_3.3SiO_2$ (7:9:3) (Gossner & Mussgnug, 1928). The compositions of sapphirines from this study are listed in Table 7 and plotted in Fig. 1. Except for the sapphirine composition in run 380-4, they show a SiO_2-enriched and Al_2O_3-depleted character similar to the sapphirine compositions reported by Grew (1981) from pegmatites of Enderby Land, Antarctica.

Schreyer & Seifert (1969) suggested that increasing pressure extends the solid solution in sapphirine to less aluminous compositions. In a result consistent with this suggestion, Taylor (1973) found a restricted range of sapphirine compositions very close to the 2:2:1 composition in equilibrium with liquids in the $MgO–Al_2O_3–SiO_2$ system at 1·5 GPa. Our data at 2·0 GPa show a wider range of sapphirine compositions approximately centered on the 2:2:1 composition but extending to both higher and lower Al_2O_3 contents (Fig. 1). In general,

Table 2: Quenching experiments

Run	Mixture*	*T* (°C)	Time (h)	Phases†
380-5	60An40En	1460	24	*gl + sa + en*
378-7	60An40En	1440	24	*gl + sa + en*
374-7	60An40En	1420	57·5	*gl + sa + en + gt + di*
380-3	80An20En	1470	8	*gl + cor*
380-4	80An20En	1450	8	*gl + sa + sp + an*
380-6‡	AFQ-20	1370	24	*gl + en + qz + an*
376-8	AFQ-20	1350	48	*gl + en + qz + an + di*
380-7	AFQ-21	1490	8	*gl + en + sp*
380-10	AFQ-21	1450	8	*gl + en + sp + di*
377-18	AFQ-22	1540	6	*gl + fo*
381-1	AFQ-22	1520	6	*gl + fo*
378-17	AFQ-22	1500	8	*gl + fo + en + sp*
378-18	AFQ-22	1480	8	*gl + fo + en + sp + di*
379-2‡	AFQ-23	1360	24	*gl + qz + an + en*
379-11	AFQ-25	1430	10	*gl + sa*
380-12	AFQ-25	1410	12	*gl + sa + di + an*
380-15	AFQ-26	1450	24	*gl + an*
381-5	AFQ-26	1410	24	*gl + an + qz*
380-16	AFQ-26	1390	24	*gl + an + qz + en*
381-8	AFQ-28	1420	6	*gl + cor + an + sa*
382-1	AFQ-28	1400	12	*gl + cor + an + sa*
383-2	AED-52	1490	8	*gl*
383-4	AED-52	1470	23	*gl + sp*
381-9	AED-52	1450	8	*gl + sp*
383-5	AED-52	1430	17	*gl + sp + di*
381-10	AED-54	1470	8	*gl*
381-12	AED-54	1450	8	*gl + di + (px)*
382-4	AED-54	1430	24	*gl + sa + di*
372-11	GS-0	1510	8	*gl + en + sp + (px)*
373-1	GS-0	1490	8	*gl + en + sp + (px)*
378-9	GS-0	1475	24	*gl + en + sp + (px)*
375-1	GS-0	1460	50	*gl + en + sa + di + (px)*
378-12‡	GS-6	1360	24	*gl + qz + an + en*
378-13‡	GS-8	1390	24	*gl + sa + en + an*
374-3	GS-11	1430	50	*gl + sa*
375-16	GS-11	1410	50	*gl + sa + gt + di*
375-17	GS-11	1370	51	*gl + di + en + an*
381-14	CMAS-4	1470	8	*gl*
381-15	CMAS-4	1450	8	*gl + di + en*
379-12	CMAS-5	1500	6	*gl*
379-13	CMAS-5	1480	8	*gl + en + di*
376-13	CMAS-5	1460	48	*gl + en + di*
376-15	CMAS-5	1440	48	*gl + en + di + sa*
376-16	CMAS-5	1420	48	*gl + en + di + sa*
376-17	CMAS-5	1400	48	*en + di + sa*
381-16	CMAS-7	1470	22	*gl*
381-17	CMAS-7	1450	24	*gl + di*

Table 2: continued

Run	Mixture*	*T* (°C)	Time (h)	Phases†
381-18	CMAS-7	1430	24	*gl* + *di* + *en*
382-7	CMAS-9	1470	24	*gl* + *qz* + *di*
382-8	CMAS-9	1430	24	*gl* + *qz* + *di*
382-10	CMAS-10	1440	24	*gl*
382-11	CMAS-10	1420	24	*gl* + *di*
382-12	CMAS-10	1400	24	*gl* + *di* + *en*
382-14	CMAS-11	1470	6	*gl*
382-15	CMAS-11	1450	7	*gl* + *di*
379-15	CMAS-12	1380	26	*gl*
379-16	CMAS-12	1360	48	*gl* + *qz* + *en* + *di* + *an*
379-17	CMAS-12	1350	48	*gl* + *qz* + *en* + *di* + *an*
379-18	CMAS-12	1340	50	*qz* + *en* + *di* + *an*
383-9	CMAS-13	1500	8	*gl*
383-11	CMAS-13	1480	21	*gl* + *di*
383-12	CMAS-13	1460	9	*gl* + *di* + *sp*
382-16	CMAS-14	1450	8	*gl*
383-13	CMAS-14	1430	7	*gl* + *an*
382-17	CMAS-14	1410	8	*gl* + *an* + *di*
383-14	CMAS-14	1390	8	*gl* + *an* + *di*
383-15	CMAS-15	1420	24	*gl*
383-16	CMAS-15	1400	27	*gl* + *gt* + *di* + *en*
383-17	CMAS-15	1380	24	*gl* + *di* + *en* + *an*
384-1	CMAS-16	1430	7	*gl*
384-2	CMAS-16	1410	8	*gl* + *en*
384-3	CMAS-16	1390	23	*gl* + *en*
384-4	CMAS-16	1370	24	*gl* + *en* + *di* + *an*
384-5	CMAS-17	1500	8	*gl*
384-6	CMAS-17	1480	8	*gl* + *fo*
384-7	CMAS-17	1460	12	*gl* + *sp* + *di* + *en*
388-7	CMAS-18	1500	8	*gl*
384-8	CMAS-18	1480	17	*gl* + *sp*
384-9	CMAS-18	1460	16	*gl* + *sp* + *di*
384-10	CMAS-18	1440	8	*gl* + *sp* + *di* + *sa*
384-11	CMAS-19	1460	8	*gl*
384-12	CMAS-19	1440	19	*gl* + *di*
384-13	CMAS-19	1400	15	*gl* + *di* + *an*

*For example, the designation 60An40En indicates the composition 60% $CaAl_2Si_2O_8$, 40% $MgSiO_3$, in wt %. (See Table 1 for compositions of mixtures labeled differently.)
†Phase abbreviations: *an*, anorthite; *cor*, corundum; *di*, diopside; *en*, enstatite; *fo*, forsterite; *gl*, glass; *gt*, garnet; *qz*, quartz; *sa*, sapphirine; *sp*, spinel; (*px*), pyroxene quench crystals.
‡Run results from Liu & Presnall (1990).

sapphirines that are higher in SiO_2 and lower in Al_2O_3 are in equilibrium with liquids that are similarly silica enriched and alumina depleted. Other coexisting mineral phases include enstatite, garnet, diopside, anorthite, spinel, and corundum (Table 7).

PHASE RELATIONS

To facilitate visualization of the relatively complex liquidus phase relations, five diagrams (Figs 2–6) are used. Figure 2 shows the liquidus surface of the forsterite–anorthite–silica base of the FADS tetrahedron. This previously published diagram (Liu & Presnall, 1990) is repeated here because it is useful in clarifying the arrangement of the spinel, sapphirine, anorthite, and corundum primary phase volumes within the FADS tetrahedron that are partly obscured in the diagrams that follow.

Figure 3 shows the liquidus univariant lines and invariant points in a perspective view of the tetrahedron, and Fig. 4 shows a companion flow sheet of the univariant lines and invariant points, following the method of Chinner & Schairer (1962) and Schairer & Yoder (1969). To facilitate cross-referencing between Figs 3 and 4, the relative positions of the invariant points in the flow sheet (Fig. 4) are oriented as closely as possible to the arrangement in composition space shown in Fig. 3. The locations (Table 8) of five of the quaternary liquidus invariant points, F, R, A, C, and T, are determined by a combination of microprobe analysis of glasses and identification of primary phases for bracketing starting compositions. Given these five points, the existence and approximate locations of five additional invariant points are inferred (Table 8) and partly constrained by quenching data in Table 2. Lines I–M, A–M, and A–B are also partly constrained by glass analyses in Table 3 (runs 378-13, 374-7, and 380-4, respectively). As univariant lines inside the tetrahedron are straight within experimental uncertainty, each invariant point must lie within the tetrahedral composition volume formed by the four invariant points with which it is connected by univariant lines. Conformance to this requirement was confirmed algebraically for each invariant point, and in some cases, small adjustments to the invariant point compositions were required.

Five univariant lines and one invariant point (S, Fig. 4) are concealed behind the opaque faceted surface partially bounded by the points, E, G, I, J, L, V, and W in Fig. 3. The divariant surfaces making up this composite opaque surface are those defined by the primary phase volumes for spinel, sapphirine, garnet, anorthite and corundum where they meet the forsterite, enstatite, diopside, and high quartz primary phase volumes (compare Figs 2 and 3). One of the concealed univariant lines joins points B and M and produces a garnet primary phase volume in the shape of a tetrahedron (see inset for Fig. 3). The other four concealed univariant lines extend from

Table 3: Glass compositions (wt %)

Mixture:	60An40En	80An20En	GS-0	GS-6	GS-8	GS-11	AFQ-20	AFQ-23	CMAS-5	CMAS-12	CMAS-12	CMAS-15
Run:	374-7	380-4	375-1	378-12*	378-13*	375-17	380-6	379-2*	376-15	379-16	379-17	383-17
T (°C):	1420	1450	1460	1360	1390	1370	1370	1360	1440	1360	1350	1380
Phases†:	*gl,sa,en,gt,di*	*gl,sa,sp,an*	*gl,en,sa,di*	*gl,qz,an,en*	*gl,sa,en,an*	*gl,di,en,an*	*gl,en,qz,an*	*gl,qz,an,en*	*gl,en,sa,di*	*gl,qz,en,di,an*	*gl,qz,en,di,an*	*gl,en,di,an*
Av. of:	6	6	6	6	6	3	6	3	7	5	3	6
SiO_2	51·00(0·33)‡	48·83(0·62)	50·52(0·48)	59·44(0·70)	53·91(0·37)	54·07(0·17)	58·07(0·20)	57·59(0·44)	51·11(0·28)	58·14(0·50)	57·31(0·07)	54·06(0·57)
Al_2O_3	22·00(0·12)	26·33(0·15)	21·46(0·24)	20·84(0·32)	22·52(0·27)	21·83(0·42)	21·36(0·17)	21·53(0·41)	21·15(0·20)	20·87(0·07)	20·72(0·15)	22·07(0·11)
MgO	12·69(0·25)	9·03(0·21)	14·75(0·11)	8·43(0·56)	10·48(0·10)	10·00(0·42)	8·48(0·10)	8·65(0·25)	13·98(0·25)	8·13(0·03)	8·48(0·06)	9·95(0·09)
CaO	14·10(0·07)	15·31(0·89)	13·83(0·58)	11·23(0·78)	12·52(0·50)	13·87(0·46)	11·97(0·53)	12·60(0·20)	13·68(0·69)	12·88(0·30)	12·83(0·27)	13·33(0·51)
Sum	99·79(0·77)	99·50(1·87)	100·56(1·41)	99·94(2·36)	99·43(1·24)	99·77(1·47)	99·88(1·00)	100·37(1·30)	99·92(1·42)	100·02(0·90)	99·34(0·55)	99·41(1·28)
An	60·15	72·20	58·23	56·89	61·80	59·71	58·35	58·54	57·75	56·94	56·91	60·58
Di	7·74	3·22	7·78	−0·89	0·51	7·21	0·85	2·91	7·91	5·42	5·58	4·63
Fo	19·68	14·80	23·07	15·02	18·23	15·15	14·54	14·09	21·85	12·42	13·09	15·97
Qz	12·42	9·78	10·91	28·98	19·45	17·93	26·25	24·46	12·48	25·22	24·42	18·82

*Run results from Liu & Presnall (1990).
†Abbreviations as in Table 2.
‡Numbers in parentheses are one standard deviation.

Table 4: Enstatite compositions (wt %)

Mixture:	60An40En	GS-0	GS-6	GS-11	AFQ-20	AFQ-20	AFQ-22	CMAS-5	CMAS-12	CMAS-15	CMAS-15	CMAS-16	CMAS-17
Run:	374-7	375-1	378-12*	375-17	380-6*	376-8	378-17	376-15	379-16	383-16	383-17	384-4	384-7
T (°C):	1420	1460	1360	1370	1370	1350	1500	1440	1360	1400	1380	1370	1460
Phases†:	*gl,sa,en,gt,di*	*gl,en,sa,di, (px)*	*gl,qz,an,en*	*gl,di,en,an*	*gl,en,qz,an*	*gl,en,qz,an,di*	*gl,fo,en,sp*	*gl,en,di,sa*	*gl,qz,en,di,an*	*gl,gt,di,en*	*gl,di,en,an*	*gl,en,di,an*	*gl,sp,en,di*
Av. of:	6	3	2	2	4	8	4	3	8	4	4	3	4
SiO_2	51·87(0·45)‡	52·29(0·23)	54·56	52·26	53·09(0·38)	53·68(0·34)	54·42(0·28)	51·96(1·11)	53·04(0·30)	51·24(0·22)	51·50(0·27)	52·35(0·69)	53·08(0·63)
Al_2O_3	13·72(0·42)	12·99(0·33)	9·86	12·85	11·77(0·43)	11·07(0·20)	9·65(0·45)	12·66(1·30)	11·66(0·57)	14·53(0·28)	14·00(0·36)	13·32(0·69)	11·02(1·00)
MgO	32·76(0·54)	33·48(0·50)	34·58	33·33	33·49(0·43)	33·88(0·60)	34·62(0·54)	33·36(0·75)	33·44(0·79)	32·42(0·34)	32·89(0·35)	32·32(0·94)	33·72(0·86)
CaO	2·03(0·32)	1·91(0·07)	1·51	1·78	1·91(0·19)	1·79(0·10)	1·64(0·24)	1·97(0·18)	1·86(0·24)	1·72(0·09)	1·88(0·20)	2·55(0·66)	2·34(0·09)
Sum	100·38(1·73)	100·67(1·13)	100·51	100·22	100·26(1·43)	100·42(1·24)	100·33(1·51)	99·95(3·34)	100·00(1·90)	99·91(0·93)	100·27(1·18)	100·54(2·98)	100·16(2·58)
Number of cations for 6 oxygens													
Si	1·738	1·748	1·822	1·754	1·780	1·797	1·821	1·750	1·782	1·724	1·728	1·752	1·784
Al(IV)	0·262	0·252	0·178	0·246	0·220	0·206	0·179	0·250	0·218	0·276	0·272	0·248	0·216
Al(VI)	0·279	0·259	0·210	0·262	0·244	0·230	0·201	0·253	0·243	0·300	0·281	0·277	0·220
Mg	1·636	1·668	1·720	1·666	1·673	1·684	1·726	1·674	1·674	1·625	1·644	1·613	1·689
Ca	0·073	0·068	0·054	0·064	0·068	0·064	0·056	0·071	0·066	0·061	0·067	0·090	0·084
Sum	3·988	3·995	3·984	3·992	3·985	3·981	3·983	3·998	3·983	3·986	3·992	3·980	3·993

*Run results from Liu & Presnall (1990).
†Abbreviations same as in Table 2.
‡Numbers in parentheses are one standard deviation.

Table 5: Diopside compositions (wt %)

Mixture:	60An40En	GS-0	GS-11	GS-11	AFQ-21	AFQ-25	CMAS-5	CMAS-12	CMAS-15	CMAS-15	CMAS-16	CMAS-17	CMAS-18
Run:	374-7	375-1	375-16	375-17	380-10	380-12	376-15	379-16	383-16	383-17	384-4	384-7	384-10
T (°C):	1420	1460	1410	1370	1450	1410	1440	1360	1400	1380	1370	1460	1440
Phases*:	*gl,sa,en,gt,di*	*gl,en,sa,di, (px)*	*gl,sa,gt,di*	*gl,di,en,an*	*gl,en,sp,di*	*gl,sa,di,an*	*gl,en,di,sa*	*gl,qz,en,di,an*	*gl,gt,di,en*	*gl,di,en,an*	*gl,en,di,an*	*gl,sp,di,en*	*gl,sp,di,sa*
Av. of:	7	3	4	1	1	3	3	10	2	3	1	2	2
SiO_2	49·08(0·29)†	49·66(0·36)	48·02(0·34)	49·12	50·28	47·41(0·50)	49·07(0·22)	50·64(0·30)	48·46	49·31(0·35)	50·44	50·70	49·20
Al_2O_3	13·94(0·30)	12·86(0·03)	15·47(0·31)	13·91	12·80	16·08(0·31)	13·21(0·09)	12·06(0·21)	15·36	14·59(0·58)	13·23	10·90	13·68
MgO	19·20(0·25)	20·16(0·30)	17·80(0·46)	19·61	22·68	15·76(0·20)	19·76(0·39)	19·08(0·21)	18·34	19·12(0·54)	19·35	22·50	20·40
CaO	17·72(0·59)	17·16(0·38)	18·95(0·38)	16·70	14·83	20·42(0·56)	17·43(0·54)	18·19(0·27)	17·16	17·33(0·64)	17·47	15·22	16·40
Sum	99·94(1·43)	99·84(1·07)	100·24(1·49)	99·34	100·59	99·67(1·57)	99·47(1·24)	99·97(0·99)	99·32	100·35(2·11)	100·49	99·32	99·68
Number of cations for 6 oxygens													
Si	1·727	1·747	1·692	1·734	1·744	1·686	1·736	1·781	1·712	1·725	1·760	1·784	1·730
Al(IV)	0·273	0·253	0·308	0·266	0·256	0·314	0·264	0·219	0·288	0·275	0·240	0·216	0·270
Al(VI)	0·305	0·280	0·334	0·312	0·267	0·360	0·287	0·280	0·351	0·326	0·304	0·235	0·296
Mg	1·007	1·057	0·934	1·032	1·173	0·835	1·042	1·000	0·966	0·997	1·006	1·179	1·069
Ca	0·670	0·646	0·715	0·631	0·551	0·778	0·661	0·685	0·649	0·649	0·652	0·573	0·618
Sum	3·982	3·983	3·983	3·975	3·990	3·973	3·990	3·965	3·966	3·972	3·962	3·987	3·983

*Abbreviations same as in Table 2.
†Numbers in parentheses are one standard deviation.

Table 6: Garnet compositions (wt %)

Mixture:	60An40En	GS-11	CMAS-15
Run:	374-7	375-16	383-16
T (°C):	1420	1410	1400
Phases*:	*gl,sa,en,gt,di*	*gl,sa,gt,di*	*gl,gt,di,en*
Av. of:	4	4	2
SiO_2	44·25(0·22)†	43·64(0·86)	44·04
Al_2O_3	24·94(0·22)	24·63(0·40)	24·84
MgO	25·52(0·40)	25·83(0·56)	25·39
CaO	6·08(0·22)	6·11(0·36)	5·81
Sum	100·79(1·06)	100·21(2·18)	100·08
Number of cations for 12 oxygens			
Si	2·996	2·978	2·986
Al(IV)	0·004	0·022	0·014
Al(VI)	1·986	1·959	1·970
Mg	2·575	2·627	2·622
Ca	0·440	0·447	0·422
Sum	8·001	8·033	8·014
Pyrope	85	85	86
Grossularite	15	15	14

*Abbreviations same as in Table 2.
†Numbers in parentheses are one standard deviation.

invariant point S (Fig. 4). Two of these lines connect S to invariant points N and U on the opaque surface and the other two connect S to points H and K in Fig. 2.

The locations of some of the phase boundaries shown in Fig. 3 are poorly constrained but representation of these boundaries as dashed lines has been avoided, to reduce confusion. The boundary surface between the high quartz volume and other volumes is constrained by data only at the forsterite–silica edge (Chen & Presnall, 1975), along line J–L (Liu & Presnall, 1990), and at point T (this study). The limit of the high quartz volume on the diopside–silica edge and the location of the diopside–corundum–high quartz piercing point on the right rear face, diopside–anorthite–silica, are taken from the preliminary diagram of Clark *et al.* (1962), although they listed no data. Estimated positions for the limits of the corundum volume at points W and L are taken, respectively, from the unreversed results of Presnall *et al.* (1978) and Liu & Presnall (1990), but these results are tentative because of sluggish reactions involving corundum. Location of a probable invariant point involving high quartz, anorthite, corundum, and diopside is unknown and indicated by a question mark.

REACTIONS AT INVARIANT POINTS

Presnall (1986) described an algebraic method for determining whether an isobaric liquidus invariant point is a

Table 7: Sapphirine compositions (wt %)

Mixture:	60An40En	80An20En	GS-0	GS-8	AFQ-28	CMAS-18
Run:	374-7	380-4	375-1	378-13*	382-1	384-10
T (°C):	1420	1450	1460	1390	1400	1440
Phases†:	*gl,sa,en,gt,di*	*gl,sa,sp,an*	*gl,en,sa,di,(px)*	*gl,sa,an,en*	*gl,cor,an,sa*	*gl,sp,di,sa*
Av. of:	7	2	3	1	3	2
SiO_2	19·10(0·54)‡	15·36	18·95(0·15)	19·07	17·03(0·33)	19·16
Al_2O_3	56·66(0·85)	62·58	56·65(0·43)	56·58	59·56(0·81)	55·80
MgO	24·16(0·40)	21·61	24·07(0·22)	23·73	23·20(0·48)	24·63
CaO	0·50(0·11)	0·58	0·50(0·08)	0·43	0·32(0·06)	0·50
Sum	100·42(1·90)	100·13	100·17(0·88)	99·81	100·11(1·68)	100·09
Number of cations for 20 oxygens						
Si	2·182	1·764	2·172	2·190	1·954	2·197
Al(IV)	3·818	4·236	3·828	3·810	4·046	3·803
Al(VI)	3·816	4·230	3·825	3·852	4·006	3·743
Mg	4·115	3·696	4·112	4·062	3·965	4·211
Ca	0·060	0·070	0·060	0·050	0·038	0·060
Sum	13·991	13·996	13·997	13·964	14·009	14·014

*Run results from Liu & Presnall (1990).
†Abbreviations same as in Table 2.
‡Numbers in parentheses are one standard deviation.

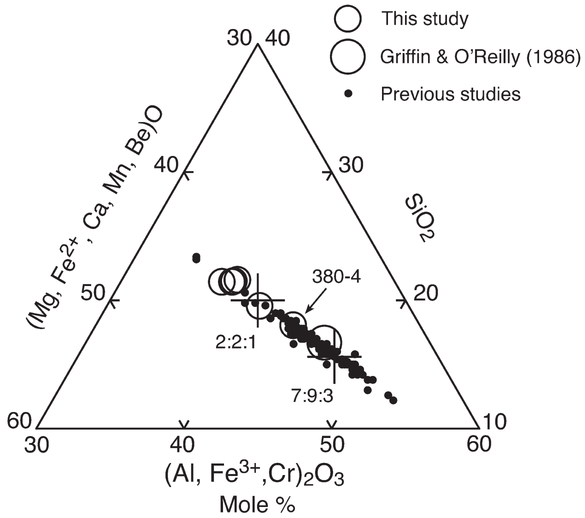

Fig. 1. Comparison of natural sapphirine compositions with those determined in this study (Table 7). Ratios shown are divalent oxides:trivalent oxides:SiO_2. Symbol size is not related to uncertainty. The data from previous studies include 146 analyses that meet two criteria: (1) an oxide sum between 99 and 101%; (2) a cation total between 13·95 and 14·05 based on 20 oxygens. The data are from Cameron (1976), Meyer & Brookins (1976), Caporuscio & Morse (1978), Grew (1980, 1981), Arima & Barnett (1984), Windley *et al.* (1984), Harley (1986), Johansson & Moller (1986), Currie & Gittins (1988), Christy (1989), Droop (1989), Grant (1989), Motoyoshi & Hensen (1989), Goscombe (1992), Kihle & Bucher-Nurminen (1992), Dasgupta & Ehl (1993), Friend *et al.* (1993), Mohan & Windley (1993), Edwin & Daniel (1994), Grew *et al.* (1994), Liati & Seidel (1994), Christy & Harley (1995), Guiraud *et al.* (1996), Tenthorey *et al.* (1996), Dawson *et al.* (1997), and Raith *et al.* (1997).

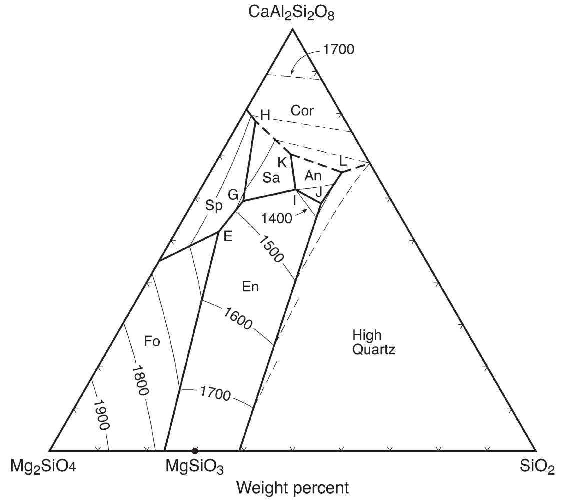

Fig. 2. Liquidus surface of the join forsterite–anorthite–quartz at 2·0 GPa, after Liu & Presnall (1990). Bold lines separate primary phase fields for forsterite (Fo), enstatite (En), high quartz, spinel (Sp), sapphirine (Sa), anorthite (An), and corundum (Cor). Fine lines are isotherms (in °C).

peritectic or eutectic point and the direction of decreasing temperature of a liquidus univariant line as it meets an invariant point. The procedure requires only a knowledge of the compositions of all the phases in equilibrium at the invariant point. For an *n*-component system, a balanced chemical equation is written involving all the $n + 1$ phases in equilibrium. Liquidus univariant lines that include the complete phase assemblage on the side of the equation not containing the liquid phase decrease in temperature away from the invariant point. All the remaining univariant lines decrease in temperature toward the invariant point. For example, at a simple ternary eutectic in which the reaction among phases A, B, C, and liquid is A + B + C = liquid, none of the phase assemblages for univariant lines coming into the eutectic contain the complete assemblage A + B + C. One of these crystalline phases will always be absent. Therefore, all of the three univariant lines decrease in temperature toward the eutectic, as is well known from classical geometrical considerations.

We use this method to characterize the invariant points and univariant lines in Figs 3 and 4. In the calculations of the reactions at invariant points, pure end-member compositions are assumed for anorthite, corundum, forsterite, quartz, and spinel. For enstatite, diopside, garnet, and sapphirine, analyzed compositions (Tables 4–7) are used. For cases in which analyzed compositions are not available for crystalline phases exactly at an invariant point, the composition of the same phase in a crystal–liquid assemblage close to the invariant point is used. Liquid compositions at invariant points are taken from Table 8. The reactions at each invariant point are listed in Table 9, and directions of decreasing temperature along univariant lines in Figs 3–4 are assigned according to these reactions. Of the five determined invariant points, F, R, A, C, and T, only T is a eutectic. All the others are peritectics (Figs 3 and 4).

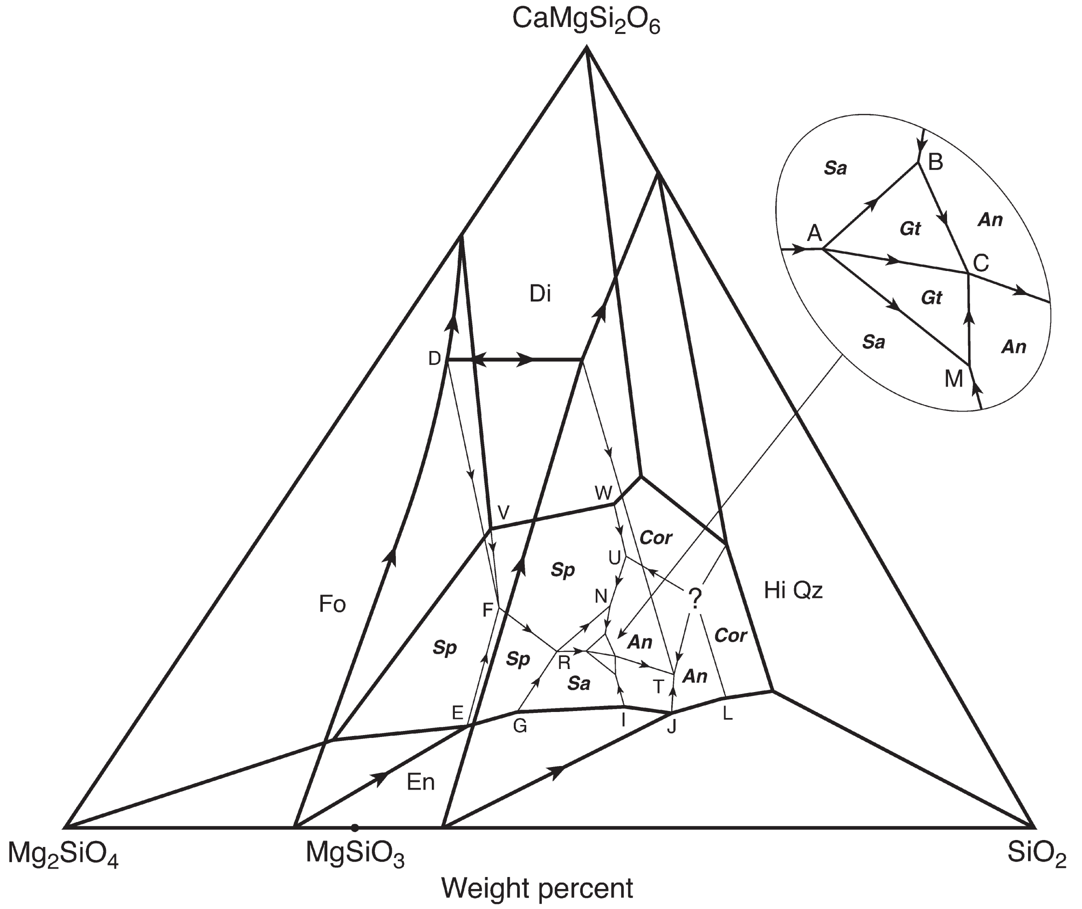

Fig. 3. Liquidus phase relations in the tetrahedron forsterite–diopside–anorthite–silica at 2·0 GPa. The anorthite apex is hidden in the rear. Bold lines are on the faces of the tetrahedron. Fine lines are in the interior. Arrows indicate directions of decreasing temperature along univariant lines. To minimize confusion of lines, the boundary surfaces in the front part of the tetrahedron are shown as transparent and those in the rear part are opaque. This hides five univariant lines and one quaternary invariant point (S, see Fig. 4) behind the faceted opaque surface. To improve clarity, point V has been moved slightly to the right from its true position and the low-Ca clinopyroxene field found by Kushiro (1969) on the front face has been omitted. This phase is not involved in any of the equilibria near the opaque surface. Bold italicized labels refer to primary phase volumes immediately behind the opaque surface. Normal labels refer to primary phase volumes in front of the opaque surface. The front face is after Kushiro (1969), the base is after Liu & Presnall (1990), the left rear face is after Presnall *et al.* (1978), and the right rear face is after Clark *et al.* (1962). Phase abbreviations are the same as in Fig. 2 with the addition of Di (diopside) and Gt (garnet).

DIOPSIDE SATURATION SURFACE

Figures 5 and 6 show the diopside saturation surface (a mosaic of divariant surfaces that define the diopside primary phase volume) projected onto the base, forsterite–anorthite–silica, of the FADS tetrahedron from the diopside apex. Figure 5 shows temperature contours and Fig. 6 shows contours of percent $CaMgSi_2O_6$ on the surface. These diagrams provide a different way of viewing some of the more important phase relations in Fig. 3 and are used here to clarify the experimental control on several of the phase boundaries. It is not possible to use these diagrams in a rigorous way to determine diopside-saturated crystallization paths because the point of projection, pure $CaMgSi_2O_6$, is not the same as the diopside compositions in equilibrium with liquids on the surface. However, these diagrams are useful for illustrating crystallization paths deduced algebraically, as discussed below.

Figure 7 shows an expanded view of the boundary lines in the upper part of Figs 5 and 6. The position of point F is from the study by Walter & Presnall (1994) and is based on a glass analysis of a run containing all the phases at the invariant point (forsterite, enstatite, diopside, spinel, liquid). Similarly, the location of point A is based on a glass analysis of a run containing sapphirine, enstatite, garnet, diopside and liquid (run 374-7, Table 3). Glass analyses are also shown for points along the R–A and C–T lines. To reduce deviations of analyzed glass compositions from the R–A line, point A is shown slightly to one side of the glass analysis that locates it. Point T is bracketed by glass analyses (Table 3) on the univariant lines C–T (runs 375-17 and 383-17)

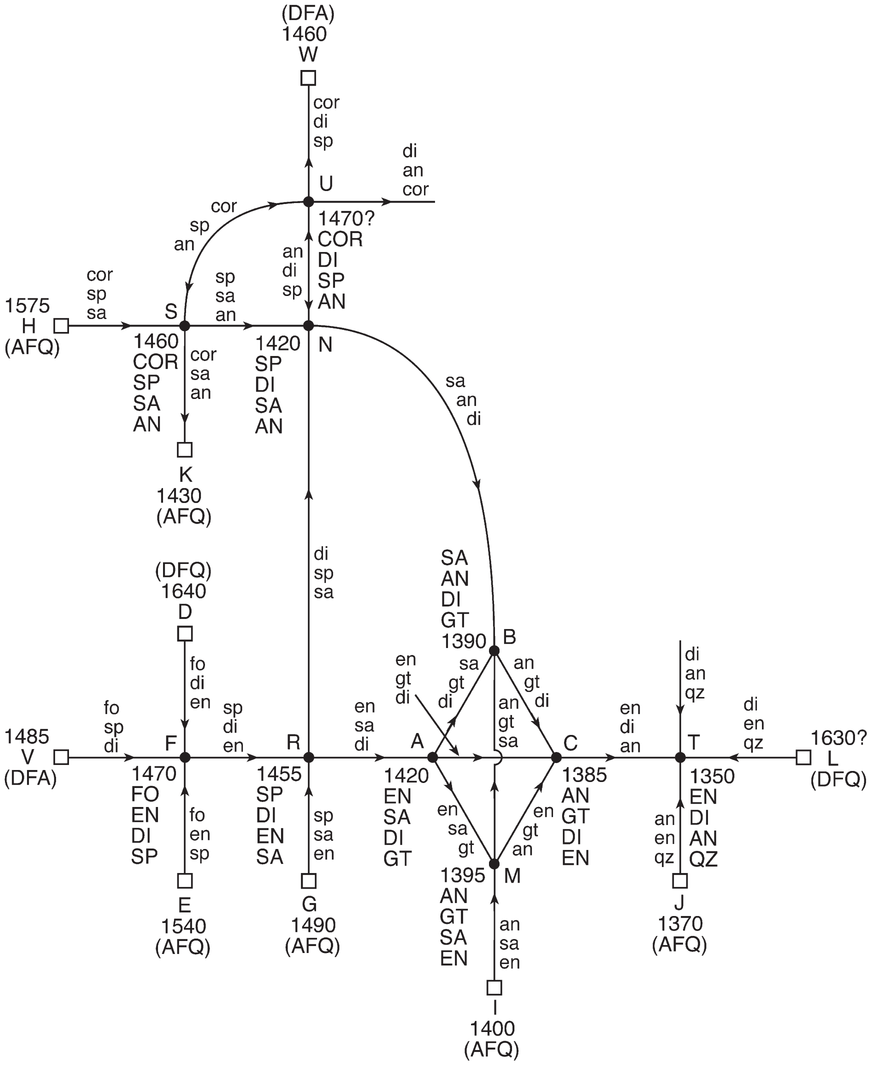

Fig. 4. Schairer diagram showing arrangement of quaternary invariant points and univariant lines in the forsterite–diopside–anorthite–quartz tetrahedron. Crystalline phases at invariant points (●) are in upper-case letters and those along univariant lines are in lower-case letters. □, intersections of univariant lines with the faces of the tetrahedron (F, forsterite; A, anorthite; D, diopside; Q, quartz). Arrows indicate directions of decreasing temperature, which is shown at each invariant point and intersection with a tetrahedral face.

and J–T (runs 378-12 and 380-6, not plotted in Fig. 7), and by two runs (379-16 and 379-17) that show all the phases at T (anorthite, enstatite, quartz, diopside, liquid). Also, Table 2 shows that quartz, enstatite, diopside, and anorthite appear simultaneously at the liquidus for mixture CMAS-12. Therefore, we locate point T between the glass analyses for 379-16 and 379-17, and slightly toward the starting composition, CMAS-12.

HIGH-PRESSURE FRACTIONAL CRYSTALLIZATION OF BASALT

In Figs 3–6, point F is a model basalt that would be produced from a spinel lherzolite (olivine + enstatite + diopside + spinel) at 2·0 GPa. If F were a eutectic, fractional crystallization at 2 GPa would not yield any evolved liquids and F would crystallize completely to a rock of its own composition. However, as F is a peritectic, some kind of fractional crystallization path must occur. Also, all other invariant points down-temperature from F are peritectics except for T, which is a eutectic. Therefore, the fractional crystallization path would be extensive. Simple inspection of the directions of decreasing temperature along the univariant lines suggests that the liquid would move along the path, F–R–A–C–T, but that a deviation might occur between A and C toward either B or M. By using the algebraic procedures of Presnall (1986, 1991), it has been shown elsewhere (Presnall, 1999) that the liquid does, in fact, move by fractional

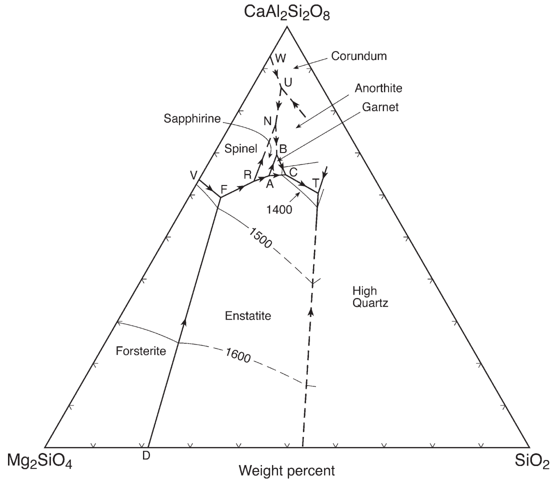

Fig. 5. Diopside-saturated liquidus surface projected from the $CaMgSi_2O_6$ apex onto the forsterite–anorthite–silica base of Fig. 3. Fine lines are temperature contours (in °C). Diopside is present in all cases in addition to the phases shown. It should be noted that the composition of diopside in equilibrium with liquids on the surface varies.

Table 8: Invariant point compositions (wt %)

Point[1]	*T* (°C)	Assemblage[2]	An	Di	Fo	Q
A[3]	1420	*gl*+*en*+*sa*+*di*+*gt*	59·6	7·7	19·8	12·9
B[4]	1390	*gl*+*sa*+*an*+*di*+*gt*	63·3	9·0	15·8	11·9
C[5]	1385	*gl*+*an*+*gt*+*di*+*en*	60·0	7·0	16·9	16·1
F[6]	1470	*gl*+*fo*+*en*+*di*+*sp*	50·0	15·7	28·7	5·6
M[4]	1395	*gl*+*en*+*an*+*gt*+*sa*	62·0	4·1	17·5	16·4
N[4]	1420	*gl*+*sp*+*di*+*sa*+*an*	68·0	11·4	12·4	8·2
R[5]	1455	*gl*+*en*+*di*+*sp*+*sa*	58·2	8·0	23·2	10·6
S[4]	1460	*gl*+*cor*+*sp*+*sa*+*an*	73	3	15	9
T[3]	1350	*gl*+*en*+*di*+*an*+*qz*	57·2	5·3	12·7	24·8
U[4]	1470	*gl*+*di*+*sp*+*cor*+*an*	71	17	7	5

[1]Letters keyed to Figs 3–8.
[2]Abbrevations as in Table 2.
[3]Composition based on analysis of glass at the invariant point.
[4]Estimated composition and temperature.
[5]Bracketed by glass analyses (Table 3) and quenching experiments (Table 2).
[6]From Walter & Presnall (1994).

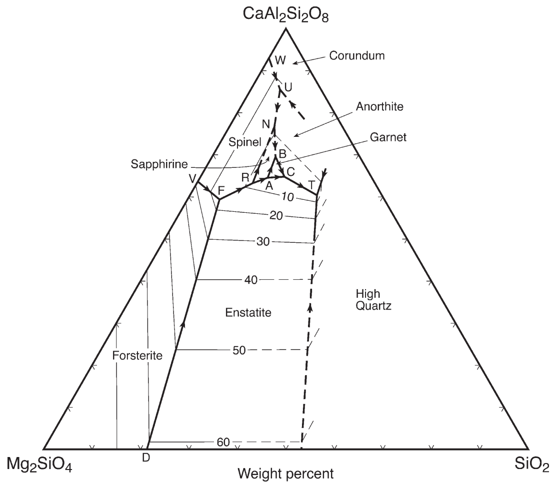

Fig. 6. Same as Fig. 5, except contours are weight percent $CaMgSi_2O_6$ in the liquid.

crystallization along the F–R–A–C–T path, and that the liquid path leaving A moves not along the A–C line but across the A–B–C surface as garnet and diopside crystallize. When the liquid reaches the B–C line, it moves down this line to C as garnet, diopside, and anorthite crystallize. As none of the univariant lines along the path show a reaction relationship, all of the phases in equilibrium with liquids on each line crystallize with decreasing temperature.

In Table 10, the composition of model basalt F is shown along with the final residual liquid produced at T and the final liquid that would occur if the fractional crystallization had occurred at 1 atm. At both pressures, SiO_2 is strongly enriched and MgO is strongly depleted. The Al_2O_3 content is slightly depleted at 1 atm and slightly enriched at 2 GPa, an effect caused by the shrinkage of the anorthite volume at higher pressures (Liu & Presnall, 1990).

The most important result of this comparison is the strong SiO_2 enrichment at 2 GPa. This result is in sharp contrast to early suggestions that enhanced crystallization of orthopyroxene from a tholeiitic basalt at high pressures leads to the production of an alkalic basalt (O'Hara & Mercy, 1963; Green & Ringwood, 1964, 1967; O'Hara, 1965; Kushiro, 1979). In Figs 3, 5, and 6, it can be seen that the initial part of the liquid path from F is characterized by crystallization of enstatite, diopside, and spinel as the liquid becomes enriched in SiO_2. The reason for this enrichment is the crystallization of spinel, a mineral observed by Green & Ringwood (1967) at 1·24 and 1·35 GPa, but not at higher pressures, and not used in their fractionation calculations. O'Hara (1965) also did not discuss the role of spinel and based his conclusions about enhanced crystallization of orthopyroxene at intermediate pressures mostly on inferred phase relations.

In Fig. 3, the spinel field at 2 GPa is very large and cuts across the forsterite–anorthite join on the base of the FADS tetrahedron, but when anorthite is replaced by albite, the spinel field is absent (Kushiro, 1968). In this case, Kushiro (1979) pointed out that fractional crystallization of forsterite and enstatite drives tholeiitic compositions across the forsterite–albite join to alkalic compositions. Spinel does not crystallize. The key issue

Table 9: Reactions at invariant points (wt)

Point*	Reactions based on phase composition data†
F	23 *en* + 68 *di* + 9 *sp* = 84 *liq* + 16 *fo*
R	37 *di* + 63 *sa* = 47 *liq* + 40 *sp* + 13 *en*
A	100 *gt* = 21 *liq* + 27 *sa* + 55 *en* + 18 *di*
C	1 *di* + 59 *en* + 41 *an* = 43 *liq* + 57 *gt*
T	18 *di* + 21 *qz* + 15 *en* + 47 *an* = 100 *liq*
Inferred reactions‡	
B	di + an + gt = liq + sa
M	an + gt = liq + sa + en
N	sa + an + di = liq + sp
S	sa + an = liq + cor + sp
U	di + cor = liq + an + sp

*Labels keyed to Figs 2–6.
†Liquid compositions from Table 8, mineral compositions from Tables 4–7 (reaction R, run 375-1; reaction A, run 374-7; reaction C, run 383-16; reaction T, run 379-16). Reactions F [data from Walter & Presnall (1994)] and A use phase composition data from single runs containing all the phases at the invariant point. Other reactions use crystalline phase compositions in equilibrium with liquids near the invariant point and are therefore less accurate. For reactions A and T, the composition of the liquid used deviates slightly from the composition in the single run as a result of constraints from other runs.
‡Phase composition data are used to determine the form of these reactions, but coefficients are not shown because the compositions of the invariant point liquids and some of the crystalline phases are not well constrained. Because the coefficients are uncertain, it is possible that even the form of some of these reactions may be incorrect.

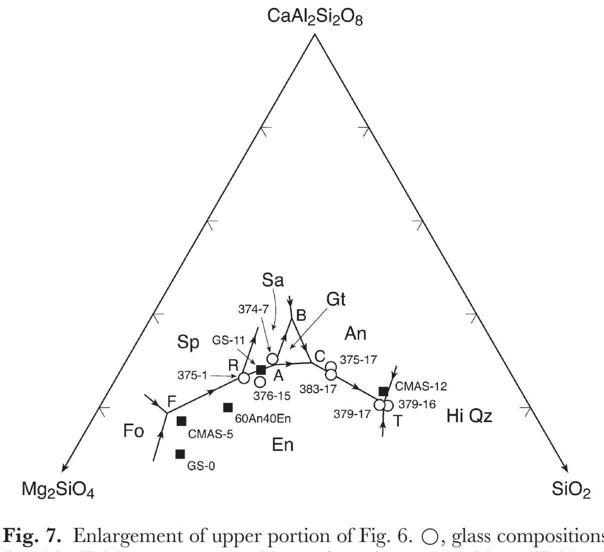

Fig. 7. Enlargement of upper portion of Fig. 6. ○, glass compositions listed in Table 3. ■, compositions of starting compositions (Table 1) that are close to the diopside-saturated liquidus surface.

Table 10: Effect of pressure on fractional crystallization

	Starting liquid*	Final liquid (1 atm)†	Final liquid (2 GPa)‡
SiO_2	48·2	62·5	57·9
Al_2O_3	18·3	15·0	21·0
MgO	19·3	8·6	8·3
CaO	14·2	13·8	12·9

*Point F, Figs 3–7.
†Composition of enstatite–diopside–anorthite–tridymite eutectic (Longhi, 1987).
‡Point T, Figs 3–7.

is whether or not spinel crystallizes from natural basaltic magmas for which the plagioclase that crystallizes is intermediate in composition between albite and anorthite. If it does, then the strong SiO_2 enrichment trend described here would occur. If it does not, then alkalic residual liquids would be expected. The issue is unresolved by existing experimental data, but it appears likely that at 2 GPa, parental tholeiitic magmas high in Na_2O would not crystallize spinel and would yield alkalic residual liquids. Those low in Na_2O would crystallize spinel and produce SiO_2-enriched residual liquids.

If our results in the CMAS system apply to natural magmas at subduction zones, then basalts generated at about 2 GPa in the mantle wedge and fractionally crystallized near the depth of generation would produce Al_2O_3- and SiO_2-enriched residual liquids similar in composition to andesites, even in the absence of volatiles. We do not advocate completely anhydrous fractionation in the mantle wedge, and Stern & Wyllie (1978) have presented data indicating that such fractionation does not exactly duplicate calc-alkaline fractionation trends at subduction zones. Nevertheless, it is interesting that the effects of high-pressure anhydrous fractionation appear in a general way to reinforce the effects of hydrous fractionation involving amphibole (Sisson & Grove, 1993).

ECLOGITES AND GARNET CLINOPYROXENITES

Rocks consisting almost entirely of garnet and clinopyroxene (eclogite if the clinopyroxene is jadeitic, garnet clinopyroxenite if it is not) are found as xenoliths in basaltic and kimberlitic eruptions (Shervais *et al.*, 1973; Irving, 1974; Griffin *et al.*, 1984; Sen, 1988; Neal *et al.*, 1990; Fung & Haggerty, 1995; Snyder *et al.*, 1997) and as bodies tectonically emplaced in orogenic zones (Dawson & Carswell, 1990). Our data bear on the common suggestion that many eclogites and garnet clinopyroxenites are magmatic cumulates. Garnet and diopside crystallize from liquids on the A–B–C surface (Figs 3, 5, and 6). The proportions of diopside and garnet that crystallize can be determined using the algebraic procedures given by Presnall (1986, 1991). A determinant is set up using the compositions of the liquids at A, B, and C (Table 8) and the garnet and diopside compositions in run 374-7 (Fig. 7, Tables 5 and 6). The resulting equation is 100A = 9di + 8gt + 31B + 52C. The coefficients in this equation show two things. First, as liquid A crystallizes, the liquid moves across the A–B–C surface to a point on the B–C line at the composition, 37% B, 63% C. Second, the proportions of minerals that crystallize are 54% diopside, 46% garnet. Thus, the phase relations support formation of at least some garnet pyroxenites and eclogites as igneous cumulates crystallized from magmas intermediate between tholeiitic basalt and andesite.

The size of the garnet primary phase volume, A–B–C–M (Fig. 3), is very small at this pressure and it increases in size with pressure. This can be seen by comparing the garnet volume in Fig. 3 with that found at 3 GPa by Milholland & Presnall (1998). Therefore, as pressure decreases from 2 GPa, the garnet volume shrinks as points A, B, C, and M converge to an invariant point in pressure–temperature space at which garnet, sapphirine, anorthite, diopside, enstatite and liquid are in equilibrium. The pressure of this invariant point is uncertain but it is probably only slightly below 2 GPa, at about 1·8–1·9 GPa. It defines the lower pressure limit for the formation of cumulate model eclogites and garnet clinopyroxenites in the CMAS system. This pressure is useful as an approximate guide for natural cumulates, but it should be used with caution because of the presence of additional components, in particular FeO and Na_2O.

O'Hara & Yoder (1967) suggested that crystallization of garnet and clinopyroxene from picritic magmas provides a mechanism for producing alkalic residual liquids from tholeiitic parents. Subsequently, O'Hara (1968) proposed that eclogite fractionation occurs from an alkalic magma. Our data, which locate the garnet–diopside surface well within the tholeiitic portion of the simplified basalt tetrahedron, do not support these suggestions at pressures in the vicinity of 2 GPa. Addition of Na_2O would be expected to extend the garnet–diopside surface toward alkalic compositions but data are not available for a quantitative discussion of this effect. Also, the garnet–diopside surface expands with pressure (Milholland & Presnall, 1998), which makes eclogite fractionation from alkalic magmas more likely at higher pressures. Thus, some cumulate garnet pyroxenites and eclogites may be crystallized from alkalic magmas at higher pressures whereas others may be crystallized from moderately fractionated tholeiitic magmas at lower pressures.

IGNEOUS SAPPHIRINE

In our earlier paper on the liquidus of the anorthite–forsterite–silica join (Liu & Presnall, 1990), we addressed two issues regarding the acceptance of sapphirine as an igneous mineral capable of crystallizing from normal mafic to modestly fractionated magmas. First, there is an apparent discrepancy between our model-system results indicating that sapphirine crystallizes from mildly mafic melts (Fig. 3) and the results of crystallization experiments on natural compositions, in which sapphirine has never been found. Second, we were aware at that time of only one report (S. A. Morse, personal communication, 1988; see also Morse & Talley, 1971) of sapphirine believed to be the result of crystallization from a mafic magma. In another occurrence, sapphirine has crystallized from a pegmatite in Enderby Land, Antarctica (Grew, 1981). In all other cases of which we are aware, sapphirine occurs in rocks that are described as metamorphic. In some of these occurrences, the sapphirine may have originally formed from a magma, but this would generally be impossible to determine with any assurance. The situation on both of these issues has not changed and we refer the reader to our earlier discussion (Liu & Presnall, 1990, pp. 740-741).

In the FADS tetrahedron, sapphirine occurs at the liquidus at 2 and 3 GPa (Milholland & Presnall, 1998). It is not present at 1 atm (Presnall *et al.*, 1979) and it was not observed at 1·0 GPa either on the forsterite–anorthite–silica base of the FADS tetrahedron (Liu & Presnall, 1990) or in some preliminary experiments performed in Presnall's laboratory within the tetrahedron (P. Thy, personal communication, 1982). The size of the sapphirine primary phase volume is smaller at 3 than at 2 GPa. Therefore, sapphirine appears to have both an upper (>3 GPa) and lower (~1·1–1·5 GPa) pressure stability limit at the liquidus for compositions within the FADS tetrahedron. This limited range of stability combined with the short interval over which sapphirine would crystallize even at 2 GPa (Fig. 3) and the tendency of high-pressure phenocrysts to dissolve on decompression severely reduce the expectation that a relict phenocryst of sapphirine would ever be brought to the surface in a lava.

Sapphirine pyroxenite from Delegate, Australia

The best hope for survival of sapphirine crystallized from a magma at high pressure would be in a cumulate xenolith brought rapidly to the surface by a subsequent eruption. Even this type of occurrence would be expected to be uncommon because of the limited range of pressure over which sapphirine is stable at the liquidus and its narrow crystallization interval (Fig. 3). A xenolith from the Delegate breccia pipes in Australia is especially interesting (Griffin & O'Reilly, 1986) and we have already discussed this xenolith in a preliminary way (Liu & Presnall, 1990). Griffin & O'Reilly (1986) interpreted this layered xenolith, which consists of clinopyroxene, plagioclase, garnet, and sapphirine, to be the result of recrystallization of an original clinopyroxene + spinel + plagioclase cumulate assemblage. More generally, Lovering & White (1969) and Irving (1974) both suggested that other layered xenoliths from the Delegate locality were formed as cumulates.

In Figs 3–6, the liquid at invariant point B is in equilibrium with diopside, anorthite, garnet, and sapphirine, the identical assemblage found in the Delegate xenolith. In addition, the Al_2O_3 contents of diopside in runs 375-16 and 380-12 (Table 5) are 15·5 and 16·1%, respectively. Both of these diopsides are in equilibrium with liquids close to B. These Al_2O_3 contents are very close to the unusually high value of 16·97% reported for the Delegate xenolith (Griffin & O'Reilly, 1986). In addition, the sapphirine in run 380-4, which is in equilibrium with a liquid close to B, has a composition significantly toward the 7:9:3 (MgO:Al_2O_3:SiO_2) composition from the other analyzed sapphirines clustering near the 2:2:1 composition (Fig. 1). This compares favorably with the Delegate sapphirine, which also lies between the 7:9:3 and 2:2:1 compositions but closer to 7:9:3 (Fig. 1). All of these similarities, combined with the absence of any petrographic evidence for an earlier mineralogy (Griffin & O'Reilly, 1986), lead us to propose that the Delegate xenolith is not recrystallized from an earlier cumulate assemblage. Instead, we believe that our experimental data provide strong evidence that the mineralogy as it exists at present is, in fact, the original cumulate assemblage.

At a pressure slightly below 2·0 GPa, perhaps 1·9–1·8 GPa, it was pointed out above that isobaric invariant points A, B, C, and M collapse to a single invariant point in *P*–*T* space. This establishes an approximate lower limit for the pressure at which the mineral assemblages in the Delegate xenolith could crystallize from a melt. Other components, most importantly iron oxide and Na_2O, may alter this result slightly. However, there is not very much room for argument based on this chemical difference because 93% of the composition of the xenolith is represented in the CMAS system. Finally, we note that the phase relations indicate a melt in equilibrium with the minerals in this xenolith intermediate between a model tholeiitic basalt (point F) and a more fractionated magma with similarities to andesite (point T).

Sapphirine norite, Wilson Lake, Labrador, Canada

S. A. Morse (personal communications, 1988 and 1998) has informed us of a possible igneous occurrence of sapphirine at Wilson Lake, Labrador, Canada. The rocks consist of hypersthene, plagioclase, and magnetite with either sapphirine or spinel. In his communication, he indicates that 'Some of the rocks are foliated but many are granular and unfoliated. The sapphirine is present in amounts up to 20+% and is often seen as independent grains in clusters with hypersthene + oxide, locally rimming these. These rocks appear to be aluminous metabasites, or in other words, reasonable candidates for sapphirine norites. Sapphirine has the same textural status as hypersthene when abundant. From the essentially gabbroic (*s.l.*) compositions and textures, they could be very credible examples of igneous sapphirine.'

In Figs 3 and 4, liquids along the univariant line M–I are in equilibrium with sapphirine, enstatite, and anorthite, essentially the assemblage observed by Morse. As we have already noted, sapphirine has not been found at the liquidus at 1·0 GPa, so this gives a rough lower limit for the pressure at which the Wilson Lake sapphirine norite crystallized, assuming it is igneous. At 2·0 GPa, liquids in equilibrium with the assemblage enstatite + anorthite + spinel (comparable with hypersthene + plagioclase + spinel in the Wilson Lake occurrence) do not exist but would be expected at lower pressures as a result of contraction of the garnet and sapphirine volumes. This suggests a rough upper limit of 2·0 GPa for crystallization of the Wilson Lake norites. As with the sapphirine pyroxenite from Delegate, the magma from which this rock crystallized would be intermediate in composition between basalt and andesite.

SUMMARY OF CONCLUSIONS

Liquidus phase relations at 2·0 GPa in the forsterite–anorthite–diopside–silica tetrahedron within the system CaO–MgO–Al_2O_3–SiO_2 indicate the following conclusions:

(1) Fractional crystallization of model basalt at 2·0 GPa leads to the production of a final residual liquid enriched in SiO_2 and Al_2O_3, and depleted in MgO, a composition with similarities to andesite. This result suggests that early experimental results indicating a fractionation trend from tholeiitic to alkalic basalt in this pressure range may apply only for tholeiitic parental magmas high in Na_2O that do not crystallize spinel. The andesitic CMAS trend may apply only to tholeiitic parental magmas low in Na_2O that crystallize spinel.

(2) The approximate lower pressure limit for the formation of garnet pyroxenites and eclogites as cumulates is 1·8–1·9 GPa.

(3) The lower pressure limit for crystallization of sapphirine at the liquidus in the CMAS system is estimated to be about 1·1–1·5 GPa and the upper pressure limit is >3 GPa.

(4) Sapphirine crystallizes from modestly fractionated liquids intermediate in composition between a model basalt and a model andesite.

(5) The assemblage sapphirine + garnet + clinopyroxene + plagioclase in a layered xenolith from Delegate, Australia (Griffin & O'Reilly, 1986) is the same assemblage as that in equilibrium with a liquidus invariant point in the CMAS system. We suggest that this is a cumulate assemblage formed at a pressure of at least 1·8–1·9 GPa.

(6) Norites at Wilson Lake, Labrador, Canada (S. A. Morse, personal communication, 1988 and 1998) have the assemblage sapphirine + hypersthene + plagioclase + magnetite, with either sapphirine or spinel. If these are igneous asemblages, phase relations in the CMAS system suggest an origin in the pressure range 1–2 GPa.

ACKNOWLEDGEMENTS

This study was carried out at the University of Texas at Dallas as part of the Ph.D. dissertation of Liu. Financial support was provided by National Science Foundation Grants EAR 84-18685 and EAR-9725900 and Texas Advanced Research Program Grant 3927 to Presnall. Liu received support from the National Science Council of Taiwan (NSC87-2116-M-003-004) during manuscript preparation. Presnall thanks Professor I. Kushiro and the Institute for Study of the Earth's Interior, Okayama University, Misasa, Japan, for financial support and a fine working environment during manuscript preparation. This paper is Contribution 897, Department of Geosciences, University of Texas at Dallas.

REFERENCES

Arima, M. & Barnett, R. L. (1984). Sapphirine bearing granulites from the Sipiwesk Lake area of the late Archean Pikwitonei granulite terrain, Manitoba, Canada. *Contributions to Mineralogy and Petrology* **88**, 102–112.

Boyd, F. R. & England, J. L. (1960). Apparatus for phase equilibrium measurements at pressures up to 50 kilobars and temperatures to 1750°C. *Journal of Geophysical Research* **65**, 741–748.

Cameron, W. E. (1976). Coexisting sillimanite and mullite. *Geological Magazine* **113**, 497–592.

Caporuscio, F. A. & Morse, S. A. (1978). Occurrence of sapphirine plus quartz at Peekskill, New York. *American Journal of Science* **278**, 1334–1342.

Cawthorne, R. G., Ford, C. E., Biggar, G. M., Bravo, M. S. & Clark, D. B. (1973). Determination of the liquid composition in experimental samples: discrepancies between microprobe analyses and other methods. *Earth and Planetary Science Letters* **21**, 1–5.

Chen, C.-H. & Presnall, D. C. (1975). The system Mg_2SiO_4–SiO_2 at pressures up to 25 kbar. *American Mineralogist* **60**, 398–406.

Chinner, G. A. & Schairer, J. F. (1962). The join $Ca_3Al_2Si_3O_{12}$–$Mg_3Al_2Si_3O_{12}$ and its bearing on the system CaO–MgO–Al_2O_3–SiO_2 at atmospheric pressure. *American Journal of Science* **260**, 611–634.

Christy, A. G. (1989). The effect of composition, temperature and pressure on the stability of the 1 Tc and 2M polytypes of sapphirine. *Contributions to Mineralogy and Petrology* **103**, 203–215.

Christy, A. G. & Harley, S. L. (1995). Titanium-bearing sapphirine in a partially melted aluminous granulite xenolith, Vestfold Hills, Antarctica: geological and mineralogical implications. *European Journal of Mineralogy* **7**, 637–653.

Clark, S. P., Jr, Schairer, J. F. & de Neufville, J. (1962). Phase relations in the system $CaMgSi_2O_6$–$CaAl_2SiO_6$–SiO_2 at low and high pressure. *Carnegie Institution of Washington Yearbook* **61**, 59–68.

Currie, K. L. & Gittins, J. (1988). Contrasting sapphirine parageneses from Wilson Lake, Labrador and their tectonic implications. *Journal of Metamorphic Geology* **6**, 603–622.

Dasgupta, S. & Ehl, J. (1993). Reaction textures in a spinel–sapphirine granulite from the Eastern Ghats, India, and their implications. *European Journal of Mineralogy* **5**, 537–543.

Dawson, J. B. & Carswell, D. A. (1990). High-temperature and ultra-high pressure eclogites. In: Carswell, D. A. (ed.) *Eclogite Facies Rocks*. Glasgow: Blackie, pp. 315–349.

Dawson, B., Harley, S. L., Rudnick, R. L. & Ireland, T. R. (1997). Equilibration and reaction in Archaean quartz–sapphirine granulite xenoliths from the Lace kimberlite pipe, South Africa. *Journal of Metamorphic Geology* **15**, 253–266.

Droop, G. T. R. (1989). Reaction history of garnet–sapphirine granulites and conditions of Archaean high-pressure granulite-facies metamorphism in the Central Limpopo Mobile Belt, Zimbabwe. *Journal of Metamorphic Geology* **7**, 383–403.

Edwin, G. & Daniel, K. (1994). Sapphirine–quartz and sapphirine–corundum assemblages in metamorphic rocks associated with the Semail Ophiolite (United Arab Emirates). *Contributions to Mineralogy and Petrology* **116**, 398–410.

Friend, C. R. L., Janardhan, A. S. & Shadakshara, S. N. (1993). A retrogressive sapphirine–cordierite–talc paragenesis in a spinel–orthopyroxenite from southern Karnataka, India. *Mineralogical Magazine* **57**, 273–288.

Fung, A. T. & Haggerty, S. E. (1995). Petrography and mineral compositions of eclogites from the Koidu kimberlite complex, Sierra Leone. *Journal of Geophysical Research* **100**, 20451–20473.

Gossner, B. & Mussgnug, F. (1928). Vergleichende Röntgenographische Untersuchung von Magnesiumsilikaten. *Neues Jahrbuch für Mineralogie, Geologie und Paläontologie, Beilage-Band Abteilung A* **58**, 213–252.

Goscombe, B. (1992). Silica-undersaturated sapphirine, spinel and kornerupine granulite facies rocks, NE Strangways Range, Central Australia. *Journal of Metamorphic Geology* **10**, 181–201.

Grant, S. M. (1989). Tectonic implications from sapphirine-bearing lithologies, south-west Grenville Province, Canada. *Journal of Metamorphic Geology* **7**, 583–598.

Green, D. H. (1973). Experimental melting studies on a model upper mantle composition at high pressure under water-saturated and water-undersaturated conditions. *Earth and Planetary Science Letters* **19**, 37–53.

Green, D. H. & Ringwood, A. E. (1964). Fractionation of basalt magmas at high pressures. *Nature* **201**, 1276–1279.

Green, D. H. & Ringwood, A. E. (1967). The genesis of basaltic magmas. *Contributions to Mineralogy and Petrology* **15**, 103–190.

Grew, E. S. (1980). Sapphirine + quartz association from Archean rocks in Enderby Land, Antarctica. *American Mineralogist* **65**, 821–836.

Grew, E. S. (1981). Surinamite, taaffeite, and beryllian sapphirine from pegmatites in granulite-facies rocks of Casey Bay, Enderby Land, Antarctica. *American Mineralogist* **66**, 1022–1033.

Grew, E. S., Pertsev, N. N., Yates, M. G., Christy, A. G., Marquez, N. & Chernosky, J. V. (1994). Sapphirine + forsterite and sapphirine + humite-group minerals in an ultra-magnesian lens from Kuhi-lal, SW Pamirs, Tajikistan: are these assemblages forbidden? *Journal of Petrology* **35**, 1275–1293.

Griffin, W. L. & O'Reilly, S. Y. (1986). Mantle-derived sapphirine. *Mineralogical Magazine* **50**, 635–640.

Griffin, W. L., Wass, S. Y. & Hollis, J. D. (1984). Ultramafic xenoliths from Bullenmerri and Gnotuk maars, Victoria, Australia: petrology of a sub-continental crust–mantle transition. *Journal of Petrology* **25**, 53–87.

Guiraud, M., Kienast, J. R. & Rahmani, A. (1996). Petrological study of high-temperature granulites from In Ouzzal, Algeria: some implications on the phase relationships in the FMASTOCr system. *European Journal of Mineralogy* **6**, 1375–1390.

Harley, S. L. (1986). A sapphirine–cordierite–garnet–sillimanite granulite from Enderby Land, Antarctica: implications for FMAS petrogenetic grids in the granulite facies. *Contributions to Mineralogy and Petrology* **94**, 452–460.

Irving, A. J. (1974). Geochemical and high pressure experimental studies of garnet pyroxenite and pyroxene granulite xenoliths from the Delegate basaltic pipes, Australia. *Journal of Petrology* **15**, 1–40.

Jaques, A. L. & Green, D. H. (1979). Determination of liquid compositions in experimental, high pressure melting of peridotite. *American Mineralogist* **64**, 1312–1321.

Jaques, A. L. & Green, D. H. (1980). Anhydrous melting of peridotite at 0–15 kb pressure and the genesis of tholeiite basalts. *Contributions to Mineralogy and Petrology* **73**, 287–310.

Johansson, L. & Moller, C. (1986). Formation of sapphirine during retrogression of a basic high-pressure granulite, Roan, Western Gneiss Region, Norway. *Contributions to Mineralogy and Petrology* **94**, 29–41.

Kihle, J. & Bucher-Nurminen, K. (1992). Orthopyroxene–sillimanite–sapphirine granulites from the Bamble granulite terrane, southern Norway. *Journal of Metamorphic Geology* **10**, 671–683.

Kushiro, I. (1968). Compositions of magmas formed by partial zone melting of the earth's upper mantle. *Journal of Geophysical Research* **73**, 619–634.

Kushiro, I. (1969). The system forsterite–diopside–silica with and without water at high pressures. *American Journal of Science* **267A**, 269–294.

Kushiro, I. (1979). Fractional crystallization of basaltic magma. In: Yoder, H. S., Jr (ed.) *The Evolution of the Igneous Rocks, Fiftieth Anniversary Perspectives*. Princeton, NJ: Princeton University Press, pp. 171–203.

Liati, A. & Seidel, E. (1994). Sapphirine and hogoomite in overprinted kyanite-eclogites of central Rhodope, N. Greece: first evidence of granulite-facies metamorphism. *European Journal of Mineralogy* **6**, 733–738.

Liu, T.-C. & Presnall, D. C. (1990). Liquidus phase relationships on the join anorthite–forsterite–quartz at 20 kbar with applications to basalt petrogenesis and igneous sapphirine. *Contributions to Mineralogy and Petrology* **104**, 735–742.

Longhi, J. (1987). Liquidus equilibria and solid solution in the system $CaAl_2Si_2O_8$–Mg_2SiO_4–$CaSiO_3$–SiO_2 at low pressure. *American Journal of Science* **287**, 265–331.

Lovering, J. F. & White, A. J. R. (1969). Granulitic and eclogitic inclusions from basic pipes at Delegate, Australia. *Contributions to Mineralogy and Petrology* **21**, 9–52.

Meyer, H. O. A. & Brookins, D. G. (1976). Sapphirine, sillimanite and garnet in granulite xenoliths from Stockdale kimberlite, Kansas. *American Mineralogist* **61**, 1194–1202.

Milholland, C. S. & Presnall, D. C. (1998). Liquidus phase relations in the CaO–MgO–Al_2O_3–SiO_2 system at 3·0 GPa: the aluminous pyroxene thermal divide and high pressure fractionation of picritic and komatiitic magmas. *Journal of Petrology* **39**, 3–27.

Mohan, A. & Windley, B. F. (1993). Crustal trajectory of sapphirine-bearing granulites from Ganguvarpatti, South India: evidence for an isothermal decompression path. *Journal of Metamorphic Geology* **11**, 867–878.

Morse, S. A. & Talley, J. H. (1971). Sapphirine reactions in deep-seated granulites near Wilson Lake, central Labrador, Canada. *Earth and Planetary Science Letters* **10**, 325–328.

Motoyoshi, Y. & Hensen, B. J. (1989). Sapphirine–quartz–orthopyroxene symplectites after cordierite in the Archaean Napier Complex, Antarctica: evidence for a counterclockwise *P–T* path? *European Journal of Mineralogy* **1**, 467–471.

Neal, C. R., Taylor, L. A., Davidson, J. P., Holden, P., Halliday, A. N., Nixon, P. H., Paces, J. B., Clayton, R. N. & Mayeda, T. K. (1990). Eclogites with oceanic crustal and mantle signatures from the Bellsbank kimberlite, South Africa, part 2: Sr, Nd, and O isotope geochemistry. *Earth and Planetary Science Letters* **99**, 362–379.

O'Hara, M. J. (1965). Primary magmas and the origin of basalts. *Scottish Journal of Geology* **1**, 19–40.

O'Hara, M. J. (1968). The bearing of phase equilibria studies in synthetic and natural systems on the origin and evolution of basic and ultrabasic rocks. *Earth-Science Reviews* **4**, 69–133.

O'Hara, M. J. & Mercy, E. L. P. (1963). Petrology and petrogenesis of some garnetiferous peridotites. *Transactions of the Royal Society of Edinburgh* **65**, 251–314.

O'Hara, M. J. & Yoder, H. S., Jr (1967). Formation and fractionation of basic magmas at high pressures. *Scottish Journal of Geology* **3**, 67–117.

Presnall, D. C. (1966). The join forsterite–diopside–iron oxide and its bearing on the crystallization of basaltic and ultramafic magmas. *American Journal of Science* **264**, 753–809.

Presnall, D. C. (1976). Alumina content of enstatite as a geobarometer for plagioclase and spinel lherzolites. *American Mineralogist* **61**, 582–588.

Presnall, D. C. (1986). An algebraic method for determining equilibrium crystallization and fusion paths in multicomponent systems. *American Mineralogist* **71**, 1061–1070.

Presnall, D. C. (1991). Algebraic methods for determining directions of decreasing temperature along isobaric liquidus univariant lines. *Canadian Mineralogist* **92**, 687–692.

Presnall, D. C. (1999). Effect of pressure on the fractional crystallization of basaltic magma. In: Fei, Y., Bertka, C. B. & Mysen, B. O. (eds) *Mantle Petrology: Field Observations and High-Pressure Experimentation. Geochemical Society, Houston, Special Publication* **6**, 209–224.

Presnall, D. C., Dixon, J. R., O'Donnell, T. H. & Dixon, S. A. (1979). Generation of mid-ocean ridge tholeiites. *Journal of Petrology* **20**, 3–35.

Presnall, D. C., Dixon, S. A., Dixon, J. R., O'Donnell, T. H., Brenner, N. L., Schrock, R. L. & Dycus, D. W. (1978). Liquidus phase relations on the join diopside–forsterite–anorthite from 1 atm to 20 kbar; their bearing on the generation and crystallization of basaltic magma. *Contributions to Mineralogy and Petrology* **66**, 203–220.

Presnall, D. C., Simmons, C. L. & Porath, H. (1972). Changes in electrical conductivity of a synthetic basalt during melting. *Journal of Geophysical Research* **77**, 5665–5672.

Raith, M., Karmakar, S. & Brown, M. (1997). Ultra-high-temperature metamorphism and multistage decompressional evolution of sapphirine granulites from the Palni Hill Ranges, southern India. *Journal of Metamorphic Geology* **15**, 379–399.

Schairer, J. F. & Yoder, H. S., Jr (1969). Critical planes and flow sheet for a portion of the system CaO–MgO–Al_2O_3–SiO_2 having petrological applications. *Carnegie Institution of Washington Yearbook* **68**, 202–214.

Schreyer, W. & Seifert, F. (1969). High-pressure phase in the system MgO–Al_2O_3–SiO_2–H_2O. *American Journal of Science* **267A**, 173–204.

Sen, G. (1988). Petrogenesis of spinel lherzolite and pyroxenite suite xenoliths from the Koolau shield, Oahu, Hawaii: implications for petrology of the post-eruptive lithosphere beneath Oahu. *Contributions to Mineralogy and Petrology* **100**, 61–91.

Sen, G. & Presnall, D. C. (1984). Liquidus phase relations on the join anorthite–forsterite–quartz at 10 kbar with applications to basalt petrogenesis. *Contributions to Mineralogy and Petrology* **85**, 404–408.

Shervais, J. W., Wilshire, H. G. & Schwarzman, E. C. (1973). Garnet clinopyroxenite xenolith from Dish Hill, California. *Earth and Planetary Science Letters* **19**, 120–130.

Sisson, T. W. & Grove, T. L. (1993). Experimental investigations of the role of H_2O in calc-alkaline differentiation and subduction zone magmatism. *Contributions to Mineralogy and Petrology* **113**, 143–166.

Snyder, G. A., Taylor, L. A., Crozaz, G., Halliday, A. N., Beard, B. L., Sobolev, V. N. & Sobolev, N. V. (1997). The origins of Yakutian eclogite xenoliths. *Journal of Petrology* **38**, 85–113.

Stern, C. R. & Wyllie, P. J. (1978). Phase compositions through crystallization intervals in basalt–andesite–H_2O at 30 kbar with implications for subduction zone magmas. *American Mineralogist* **63**, 641–663.

Taylor, H. C. J. (1973). Melting relations in the system MgO–Al_2O_3–SiO_2 at 15 Kb. *Geological Society of America Bulletin* **84**, 1335–1348.

Tenthorey, E. A., Ryan, J. C. & Snow, E. A. (1996). Petrogenesis of sapphirine-bearing metatroctolites from the Buck Creek ultramafic body, southern Appalachians. *Journal of Metamorphic Geology* **14**, 103–114.

Walter, M. J. & Presnall, D. C. (1994). Melting behavior of simplified lherzolite in the system CaO–MgO–Al_2O_3–SiO_2–Na_2O from 7 to 35 kbar. *Journal of Petrology* **35**, 329–359.

Windley, B. F., Ackermand, D. & Herd, R. K. (1984). Sapphirine/kornerupine-bearing rocks and crustal uplift history of the Limpopo belt, Southern Africa. *Contributions to Mineralogy and Petrology* **86**, 342–358.

Yoder, H. S., Jr & Tilley, C. E. (1962). Origin of basalt magmas: an experimental study of natural and synthetic rock systems. *Journal of Petrology* **3**, 342–532.